processes

MDPI

Article

Tributary Channel Width Effect on the Flow Behavior in Trapezoidal and Rectangular Channel Confluences

Aliasghar Azma [1] and Yongxiang Zhang [2,*]

[1] College of Architecture and Civil Engineering, Beijing University of Technology, Beijing 100124, China; aa.azma1990@emails.bjut.edu.cn

[2] Institute of Water Resources and Engineering Municipal Engineering Department, College of Civil Engineering and Architecture, Beijing University of Technology, Beijing 100124, China

* Correspondence: yxzhang@bjut.edu.cn

Received: 5 September 2020; Accepted: 21 October 2020; Published: 24 October 2020

Abstract: Channel confluences happen commonly in water transport networks and natural rivers. Utilizing a 3D CFD code, a series of numerical simulations were performed using a large eddy simulation turbulence model to investigate the effect of the variations in tributary channel width and the transverse geometrical shape of the main channel on the flow parameters and vertical structure in a T-shape confluence. The code was calibrated using the experimental data from the literature. Flow parameters were considered in ratios of tributary width to the main channel width in trapezoidal and rectangular channels. Results indicate that decreasing the width ratio of the tributary channel to the main channel significantly affects the flow structure in the confluence. Generally, it increases the width and length of the main recirculation zone. It also increases the maximum velocity near the bed, especially in cases with a trapezoidal shape. Besides, it highly affects the structure and formation of the recirculation zone in trapezoidal channels.

Keywords: channel confluence; flow structure; the separation zone

1. Introduction

Confluences are important structures due to the highly turbulent and complex flow structure forms at the junction section. Different geometrical and hydraulic parameters including planform, cross-sectional shape, bed-level concordance or discordance, the momentum flux ratio [1–5] and the density difference between streams [6] affect the hydraulic and fluvial processes within and around the channel confluences. The main patterns of the hydrodynamic behavior of confluences includes a large separation zone at the downstream corner of the confluence, a stagnation zone at upstream corner, a shear layer at the interface of tributary flow with the main channel flow and a flow recovery zone at the downstream end of the channel confluence [7].

An increased flow velocity as well as a drop in flow surface, could also be considered among the main processes at the confluence [8]. A comprehensive investigation of the three-dimensional flow structure around hydraulic structures could provide a thorough understanding of the sediment transport and flow characteristics that affect the performance of such structures [9].

Generally, researchers, including Taylor [10], Webber and Greated [11], Shumate [12], and Mignot et al. [13], have emphasized the discharge ratio of side-channel to the main channel (momentum flux ratio) as the key parameter controlling the flow structure. In natural and man-made channels, especially in simple channels such as drainage canals, the separation zone is a dominant component of the flow structure due to the sharp-edged form of the canals and their bed-level concordance [11,12]. The separation zone is the preferred location for sediment deposition. It also

reduces the effective width of the channel resulting in an increased velocity along the channel as well as the shear stress on the bed. Consequently, it affects the head loss along the confluence [2].

Zhang et al. [14] utilized the k-ω turbulence model, and the Reynolds averaged Navier–Stokes equations to study the effect of the ratio of tributary flow to the total downstream channel discharge on the shape and size of the formed separation zone, and the coefficient of contraction for a 90° open-channel with equal width. They concluded that smaller discharge ratios of the tributary to the main channel might result in a more uniform distribution of flow and velocity profiles over the downstream channel. They also stated that the shape index of the recirculation zone in the main channel remains almost constant despite the variations in length and width of it. Zeng and Li [15] modeled the flow in an open-channel confluence utilizing a hybrid RANS–large-eddy simulation (LES) model. The accurate and precise estimate of the flow using the proposed model compared to those provided by RANS indicated the strength of this model. Schindfessel et al. [16] scrutinized the flow patterns in a confluence with a large fraction (90%<) of the total flow comes from the tributary channel. Their results indicate that the tributary flow collides with the opposite wall in the case of dominant tributary discharge, resulting in forming a large recirculating zone in the upstream channel.

Sharifipour et al. [17] used a variant of the k-ω model to estimate the effect of side-channel width on the flow properties in the main channel. It was found that varying the width ratio between the side channel and the main channel from 0.5 to 2 may decrease the governance of tributary flow on the characteristics of flow in the main channel. Ramos et al. [18] compared the preciseness of two techniques, including flat and rigid-lid for simulation of flow surface utilizing the LES turbulence model. Ramos et al. [19] investigated the effect of bed elevation discordance and the flow structure's discordance in a T confluence. They suggest significant variations in the form and size of the recirculation zone due to bed-level variations. Schindfessel et al. [2] studied the effect of the main channel cross section shape on the flow behavior in a T-shape junction. Their results indicate that the geometrical properties of the main channel highly affect the dimensions of the recirculation zone. It is mainly due to the lateral currents directed into the separation zone. Besides, it is found that a reduced separation zone also shows a reduced head loss.

Reviewing the literature, it could be concluded that there is no considerable description of the different aspects of flow behavior in confluences with geometries other than rectangular cross-sections. In fact, the majority of studies, including Azma and Zhang [20], have focused on the flow behavior in cross-sections of simple rectangular channels in different hydraulic and discharge conditions. Besides, the effect of the tributary channel's width ratio to the main channel on the flow characteristics is not fully investigated. Consequently, the present study investigates the differences between flow patterns induced by different tributary channel width ratios in constant discharges from tributary and main channel in rectangular channels. Afterward, the effect of discharge variation and tributary channel width ratio on the flow structure in trapezoidal main channels are discussed in detail. Finally, a short comparison of the differences of the 3D behavior of flow in rectangular and trapezoidal main channels is presented.

2. Materials and Methods

2.1. Laboratory Model

In this study, the CFD code is calibrated using the experimental data of Webber et al. (2001). The experimental facilities consisted of a main channel 21.95 m long, 0.91 m wide (W_{mc}), and 0.51 m high (h_{mc}), in addition to a side-channel with the height and width the same as that for main channel but 3.66 m long. A total discharge of Q_t = 0.17 m^3/s with h = 0.296 m, originating a Froude number equal to Fr_t = 0.37, with 75% of the flow (q* = 0.75) coming from the tributary (as a critical condition for simulation), was used in the calibration test. Measurement facilities include a Sontek ADV with ±1% accuracy, a sampling time of 60 seconds in each point and a sampling rate of 10 Hz.

2.2. Numerical Model

The FLOW-3D CFD code was opted as a solver of the Navier–Stokes equation to estimate the three-dimensional flow parameters at the confluence.

2.3. Governing Equations

Governing equations for the model are momentum and continuity. The continuity equation, in the Cartesian coordinates could be described as:

$$V_{\mathrm{F}}\frac{\partial \rho}{\partial t} + \frac{\partial}{\partial x}(uA_x) + \frac{\partial}{\partial y}\Big(vA_y\Big) + \frac{\partial}{\partial z}(wA_z) = \frac{R_{\mathrm{sor}}}{\rho} \tag{1}$$

where u, v, and w are the components of velocity in the x, y, and z directions, respectively; A_x, A_y, and A_z are the fractions of the surface flow in the x, y, and z, respectively; V_{F} is the fraction of the flow volume; ρ is the density of fluid; t is time, and R_{sor} is the mass source. Equation (2) describes the momentum equation:

$$\begin{aligned}
&\tfrac{\partial u}{\partial t} + \tfrac{1}{V_{\mathrm{F}}}\Big(uA_x\tfrac{\partial u}{\partial x} + vA_y\tfrac{\partial u}{\partial y} + wA_z\tfrac{\partial u}{\partial z}\Big) = -\tfrac{1}{\rho}\tfrac{\partial \rho}{\partial x} + G_x + f_x\\
&\tfrac{\partial v}{\sigma t} + \tfrac{1}{V_{\mathrm{F}}}\Big(uA_x\tfrac{\partial v}{\partial x} + vA_y\tfrac{\partial v}{\partial y} + wA_z\tfrac{\partial v}{\partial z}\Big) = -\tfrac{1}{\rho}\tfrac{\sigma \rho}{\partial y} + G_y + f_y\\
&\tfrac{\partial w}{\partial t} + \tfrac{1}{V_{\mathrm{F}}}\Big(uA_x\tfrac{\partial w}{\partial x} + vA_y\tfrac{\partial w}{\partial y} + wA_z\tfrac{\partial w}{\partial z}\Big) = -\tfrac{1}{\rho}\tfrac{\sigma \rho}{\partial z} + G_z + f_z
\end{aligned} \tag{2}$$

where G_x G_y, and G_z are the gravity accelerations in the x, y, and z directions, respectively; f_x,f_y, and f_z are the viscous accelerations in the x, y, and z directions, respectively.

2.4. Turbulence Modeling

The large-eddy simulation (LES) model was utilized to simulate the confluence's complex turbulent flow field. The Flow-3D software adopts the standard Smagorinsky model for the subgrid-scale stresses. The filter is the mesh size. In the LES model, the effects of turbulence too small to compute are represented by an eddy viscosity, which is proportional to a length scale multiplied by a measure of velocity fluctuations on that scale. For the length scale, Flow-3D uses a geometric mean of the grid cell dimensions as follows:

$$L = (\delta x \delta y \delta z)^{\frac{1}{3}} \tag{3}$$

Velocity fluctuations are scaled by the magnitude of L times the mean shear stress. These quantities are combined into the LES kinematic eddy viscosity:

$$v_T = (cL)^2.\sqrt{2e_{ij}2e_{ij}} \tag{4}$$

where (c) is a constant having a typical value in the range of 0.1 to 0.2 and (e_{ij}) denotes the strain rate tensor components.

2.5. Boundary Conditions and Gridding

A non-uniform structured grid domain was utilized to calculate the flow in main channel and the tributary. The cells are smaller in the vicinity of the confluence to increase the accuracy of computations. Boundary conditions are discharge inflow for the main channel entrance and the tributary, constant level outflow (constant pressure) for the outlet of the downstream channel, the no-slip boundary condition for the bed, and the side boundaries of the main channel, and symmetry for the top border. Considering that two large useless domains at the sides of the lateral channel were produced due to the use of a single mesh domain, they were eliminated from calculations using void or space components to reduce the computational effort. Considering the limitations in processing power, various cell sizes were tested; however, the computational capacity restricted using cells with sides less than 3 mm.

Thus, a mesh domain, with 16-m length, 5-m width, and 0.4-m height, was considered that consisted of 4,287,400 cells, and was opted to simulate the channels. The computational grid composed of 340 cells in the x-direction, 194 in the y-direction, and 65 cells in the z-direction. As mentioned above, the cells adjacent to the borders were as small as 3*3*3 mm. The mesh size at the corners of the confluence was also determined the same as those for the simulation of boundary layers (3*3*3 mm). The plan of the mesh domain with boundary conditions, and the cross-sectional shape of the channel are plotted in Figure 1.

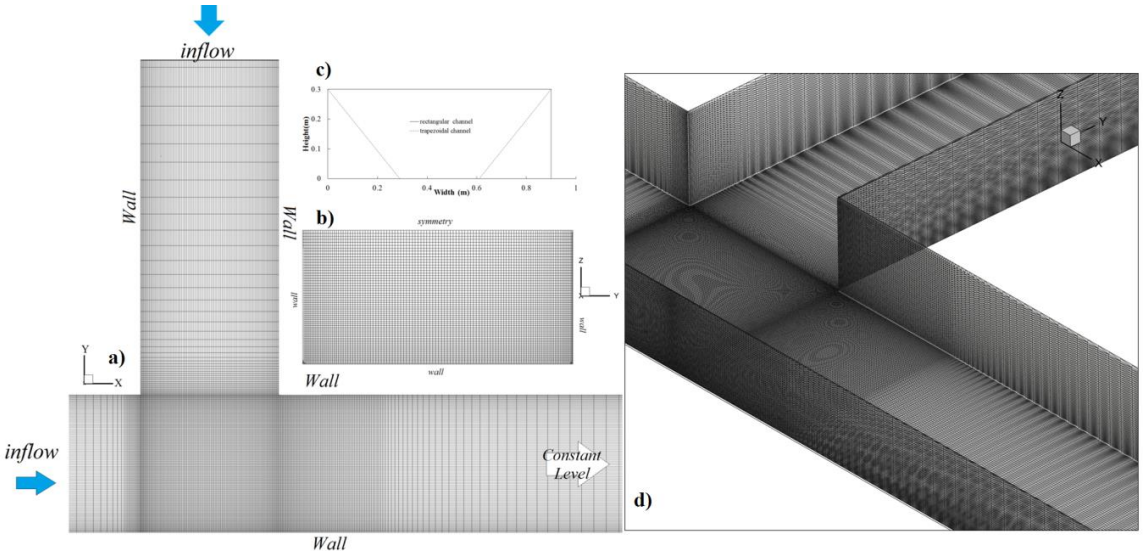

Figure 1. Plan of mesh (**a**) with boundary conditions and a cross-sectional view of mesh (**b**) and the cross-section geometries (**c**) and 3D view of the confluence and mesh domain (**d**).

2.6. Simulation Scenarios

Nine different conditions were investigated with various geometrical and discharge flow conditions. Table 1 describes the simulation parameters and discharge ratios of each test. Five cases with a rectangular main channel are considered, with 4 cases with a trapezoidal geometry. In the first step, the effect of variations in the tributary channel width (Wsc) on the flow behavior in the confluence will be investigated.

Table 1. Simulation cases.

Case No.	Geometrical Shape	$W^* = W_{sc}/W_{mc}$	Q_{mc} (m^3)	Q_{sc}	Fr_{mc}	Fr_{sc}	Fr*
0 (validation test)(validation case)	Rectangle	1	0.042	0.127	0.092	0.28	3.04
1	Rectangle	0.25	0.127	0.042	0.28	0.366	1.31
2	Rectangle	0.5	0.127	0.042	0.28	0.183	0.65
3	Rectangle	0.75	0.127	0.042	0.28	0.122	0.44
4	Rectangle	1	0.127	0.042	0.28	0.092	0.33
5	Trapezoid(1:1)	0.25	0.127	0.042	0.5	0.366	0.73
6	Trapezoid(1:1)	0.25	0.097	0.042	0.36	0.366	1.02
7	Trapezoid(1:1)	1	0.127	0.042	0.5	0.092	0.18
8	Trapezoid(1:1)	1	0.097	0.042	0.36	0.092	0.26

2.7. Model Verification

The momentum advection equation with a first-order approximation along with the implicit generalized minimal residual method (GMRES) with a maximum of 120 internal iterations in each computational step, an initial time step equal to 1E-6, and the fractional area-volume obstacle representation (FAVOR) method for estimation of the free surface were determined to calculate the

velocity and pressure field within the computational domain. The laboratory data of Webber et al. (2001) were used to validate the CFD code. The laboratory results were compared with those from four turbulence models of k-ω, k-ϵ (RNG), K-ϵ standard, and the LES. It is obvious that the LES turbulence model best presents the transverse flow patterns, which are of paramount importance in 3D spiral flows such as the present problem. Consequently the LES turbulence model with R^2 = (0.94, MAE = 0.14, and RMSE = 0.18) over K-ϵ standard model (with R^2 = 0.91, MAE = 0.17, and RMSE = 0.26), RNG (with R^2 = 0.90, MAE 0.15, and RMSE = 0.29), and k-ω (with R^2 = 0.92, MAE = 0.16, and RMSE = 0.23) was determined as the proper turbulence model. Figures 2 and 3 present a comparison of the accuracy of the estimation of the (U) velocity component and the free surface profile between the predicted and lab results.

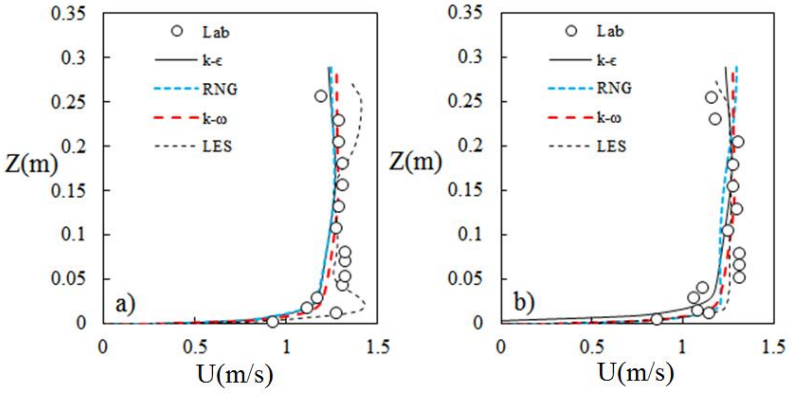

Figure 2. Velocity (U) calculations by various turbulence models at x = 8.82 (x* = 2 Wc) and (**a**) y = 0.25 Wc, and (**b**) y = 0.5 Wc.

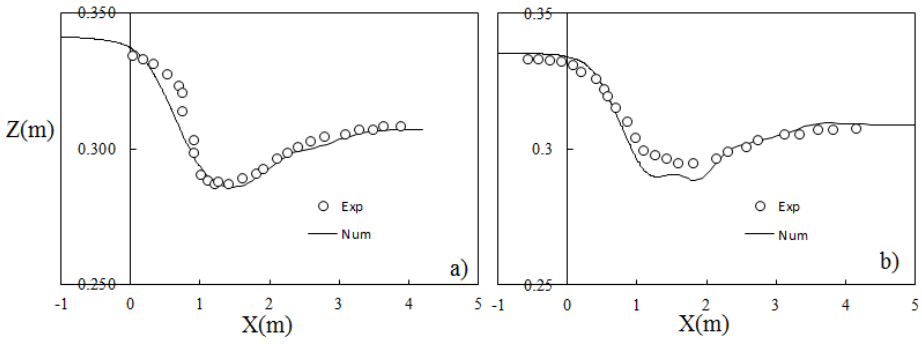

Figure 3. Comparison of measured with large-eddy simulation (LES)-simulated flow surface in (**a**) y/W = 0.167 and (**b**) y/W = 0.5.

3. Results and Discussion

3.1. Rectangular Main Channel

3.1.1. Longitudinal Velocity Distribution and Flow Patterns

The distribution of the stream-wise component of velocity (U) at the x–y plane of the confluence structure along the main channel is presented in Figure 4, respectively, for four cases including case (1) to case (4) with the width ratio of the tributary channel to the main channel (W_{sc}/W_{mc} = W*) from W* = 0.25 to 1. Results are presented in three different flow depths including $Z^* = Z/Z_0$ = 0.05 (close to bed) to 0.93 (close to water surface). Generally, results show that increasing the W* from 0.25 to 1 highly affects the 3D flow behavior at the confluence. Figure 4 shows that increasing the tributary width results in reducing the maximum velocity at the main channel downstream of the confluence. This is a direct consequence of the higher flow velocity from the tributary channel to the main channel in smaller

W* ratios, which has a similar effect as increasing tributary discharge from tributary channel (see [9,10]). On the other hand, the velocity gradient toward the recirculation zone increased as the tributary width decreased, which may result in an increased recirculation area and power. Separate high-velocity zones could be observed, especially in case (1) with W* = 0.25, which indicates a complex flow behavior induced by the transverse spiral movements of flows. Various investigations have shown that increasing the momentum flux from the side channel with constant width causes the maximum velocity zone to move downstream toward the opposite wall of the main channel (see [4,14]), yet, it was observed that reducing the tributary width resulted in a slightly different behavior [10]. Although the high-velocity zone expands toward the opposite wall, the maximum value of velocity occurs adjacent to the recirculation zone immediately downstream of the confluence section. Note that the velocity magnitude is maximum near the flow surface as expected.

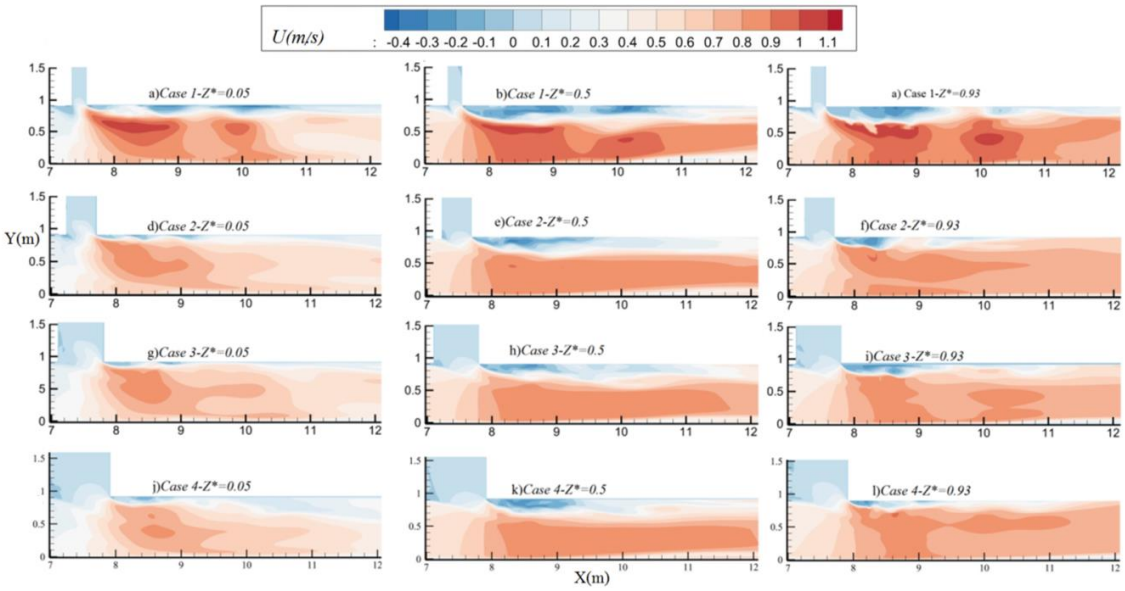

Figure 4. The distribution of the stream-wise component of velocity (U) in the rectangular channel.

Figure 5 presents the distribution of the normal component of velocity (V) over the x–y plane at the same level and conditions as those shown in Figure 4. It is observed that the maximum value of the V velocity takes place at the downstream corner of the tributary channel with the main channel and its value and gradient increases as the tributary width decreases.

In addition, the area of the stagnation zone at the upstream corner of the tributary channel with the main channel increases with decreasing the W*. It is caused by the effect of the higher downward velocity from the narrower tributary channel, which causes a higher upstream water level or backwater effect [21]. It is similar to increases in the tributary channel discharge in studies such as ref. [2] and [10]. By increasing the tributary width, this stagnation zone moves up toward the upstream wall of the tributary channel, forming a recirculation zone in the tributary channel which results in the reduction of its effective width. Note that the area of this formed recirculation zone (stagnation zone) tributary channel is maximum near the bed, where it reduced the tributary channel up to 20% resulting in a 3D upward flow at the upstream inner corner of the tributary channel (see Figures 5 and 6).

Figure 6 presents the normal component of velocity (V) over the x–y plane. A complex flow behavior with different separating planes and recirculation areas could be observed, suggesting a complex transverse flow behavior. It is indicated that the width of the recirculation zone increases as the tributary width decreases. In addition, it could be observed that the width of the plane separating the tributary flow from the main flow increases with decreasing W* from 1 to 0.25. Besides, it could be

inferred that the length and complexity of the main recirculation zone increase with the W* decreasing from 1 to 0.25, suggesting that a more complex spiral flow forms as the tributary width decreases.

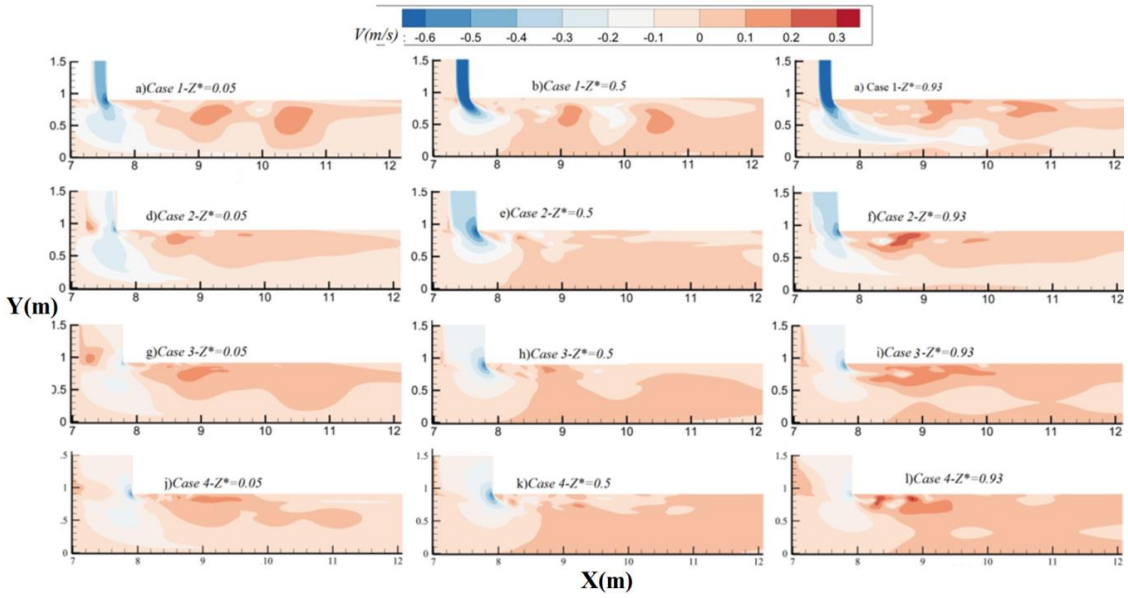

Figure 5. The distribution of the normal component of velocity (V).

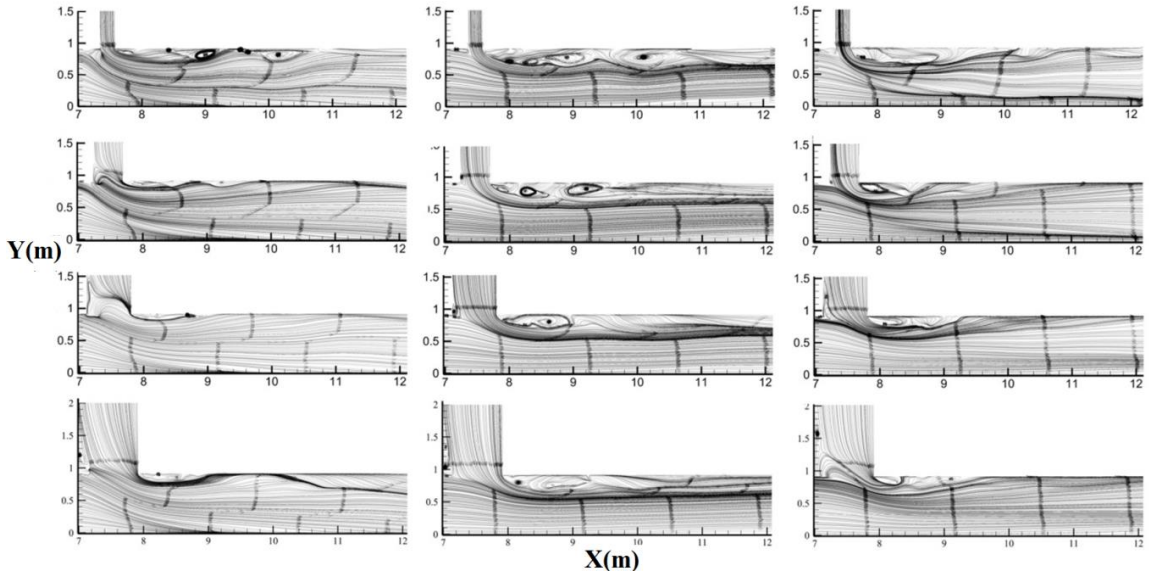

Figure 6. The effect of changing W* on the flow pattern at different elevations for various cases.

3.1.2. Transverse Velocity Distribution and Flow Patterns

In order to investigate the flow behavior in transverse planes, Figures 7 and 8 present the transverse distribution of the U component of velocity as well as the streamlines in the transverse plane (y–z) of $X^* = X/W_{mc} = 1$ and 2 starting from the downstream wall of the tributary channel. Comparing the area of the recirculation zone at X* = 1 (Figure 7a,c,e,g) shows that increasing the tributary width results in the reduction of the recirculation area at the transverse plane as well as the plan view. Additionally, it could be observed that decreasing W* amplifies the complexity and power (intensity) of the recirculation zone. It is indicated that the maximum intensity of recirculation zone in case (4) with W* = 1 is located at Z* = 0.45 while the maximum value of return flow in case (1) with W* = 0.25 happens near the flow surface, suggesting a different vertical structure for cases (1) to (4). In addition, a comparison between

the velocity distribution at X* = 1 to that for X* = 2, indicates that the area and the power of the main recirculation zone is decreased at X* = 2 compared to that of X* = 1. Yet, the main difference lies in the form and structure of the recirculation zone. Comparing Figure 7b to Figure 7h, it could be observed that in case (1), the maximum width of the recirculation area occurs at Z* = 0.8 (near the surface while occurs at Z* = 0.2 for case (4) with W* = 1.

Figure 8 presents the vertical structures formed due to the interaction of the tributary channel with the main flow at X* = 1 and 2 downstream of the confluence. Comparing the flow patterns in X* = 1 for different *W** ratios indicate that generally, three main vertical zones form in the channel; (1) a large clockwise roller at the flow surface close to the outer wall of the main channel, (2) a counter-clockwise vortex adjacent to the bed tangent to the outer wall of the channel, and (3) a group of counter-wise vortices which form the main recirculation area. Results indicate that the surface roller dissipates as the W* increases from 0.25 to 1. Besides, the counter-clockwise vortex in the lower opposite corner of the channel gradually shrinks by increasing the W* ratio. The vortex group tangent to the inner wall of the main channel has a very complex nature due to the interaction with the surface roller. It could be inferred that for case (4) where the surface roller completely vanishes, the counter-clockwise movement of the flow is the governing pattern, while for case (1) with larger surface roller the clock wise spiral movement of flow highly affects the counter-clockwise movement of the main body flow. A comparison between the flow patterns at X* = 1 and X* = 2 for the same cases indicates that the surface roller and the counter-clockwise deep vortex dissipate as the flow moves downward (see Figure 8b,d,f,h). Hence the inner wall vortex group becomes the governing flow pattern along the downstream channel, which forms a large counter-clockwise spiral movement.

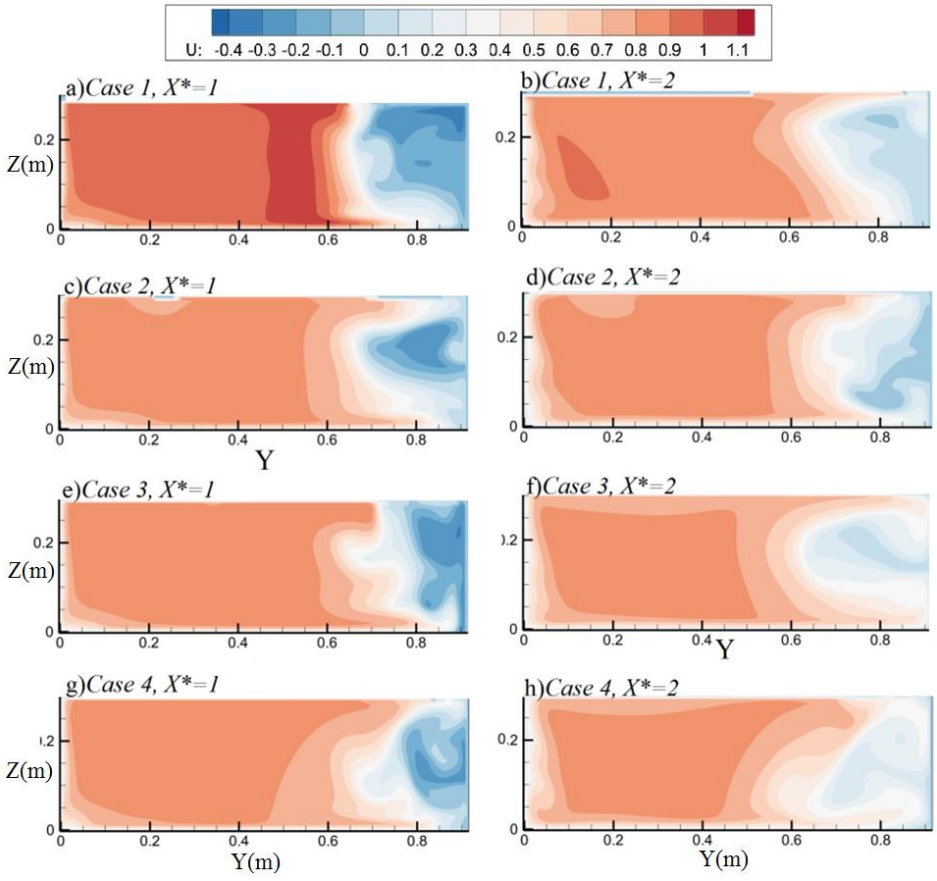

Figure 7. The effect of W* variations on the distribution of U in transverse plane.

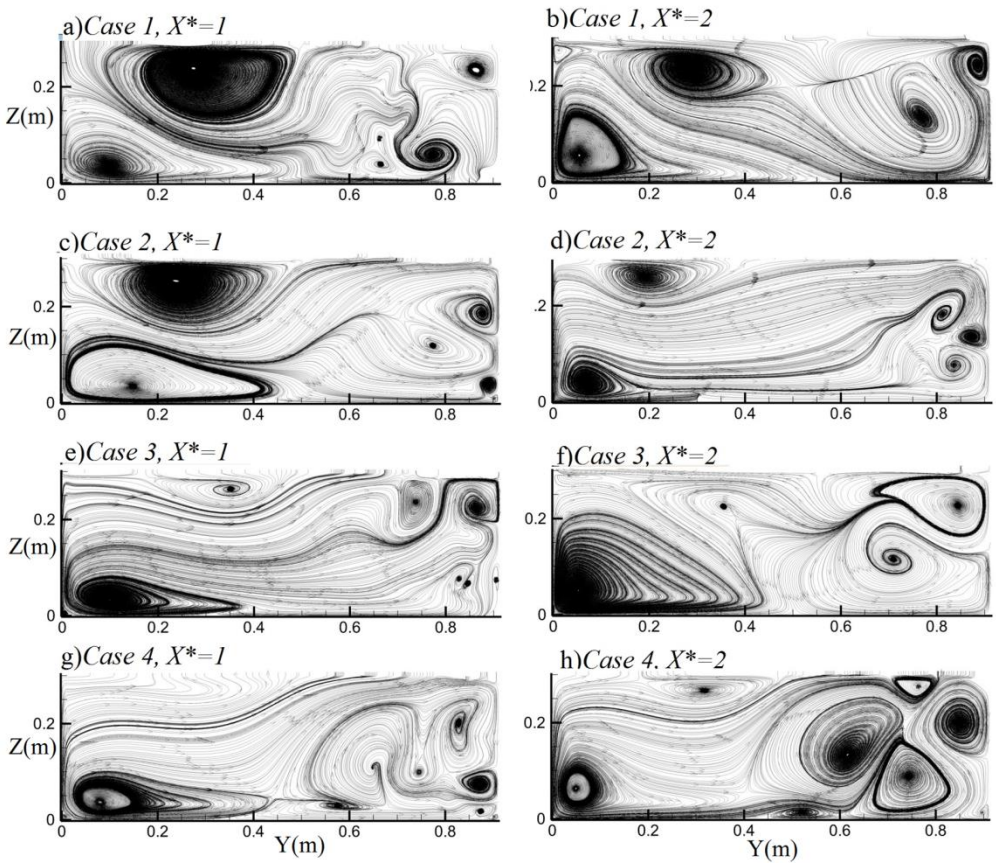

Figure 8. The effect of W* variations on the vertical structure in the transverse plane.

3.2. Trapezoidal Main Channel

3.2.1. Longitudinal Velocity Distribution and Flow Patterns

The same procedure for trapezoidal channels is performed to investigate the flow patterns in channels with trapezoidal cross-sections. Figures 9 and 10 present the distribution of the velocity components at Z* = 0.05, 0.5, and 0.93 for three cases—(5), (6), and (7). In fact, Figures 9 and 10 investigates the effect of variations in the upstream main channel discharge as well as increasing the tributary width on the distribution of stream-wise and normal components of velocity in a trapezoidal channel with the side slope of 1:1. Figure 9a–c presents the (U) velocity distribution over the channel in various elevations. It could be inferred that the area of high velocity near the bed occurs at the central line of the channel while it moves toward the left bank as the flow level increases from the bed. Note that the absolute maximum velocity occurs at the intersection point of the tributary channel with the main channel. Comparing Figure 9a–c to Figure 9d–f indicates that by decreasing the upstream flow discharge, the area of the upstream stagnation point is increased due to the decrease in the power of the upstream flow which results in higher backflow effect induced by the tributary flow. Additionally, comparing Figure 9c–f indicates that decreasing the upstream discharge resulted in an increase in area and intensity of the main recirculation zone. An interesting point in all trapezoidal channel tests is the absence of backward currents and consequently, the recirculation zone in flow altitudes lower than 0.5 from the bed. However, decreasing the upstream discharge resulted in developing the recirculation zone to depths lower than Z* = 0.5. Hence, it could be concluded that decreasing the upstream discharge (or increasing the tributary discharge) and consequently the velocity in the y-direction may result in the increase in the area of the upstream stagnation zone as well as the area, power and depth of the downstream recirculation zone (see Figure 10).

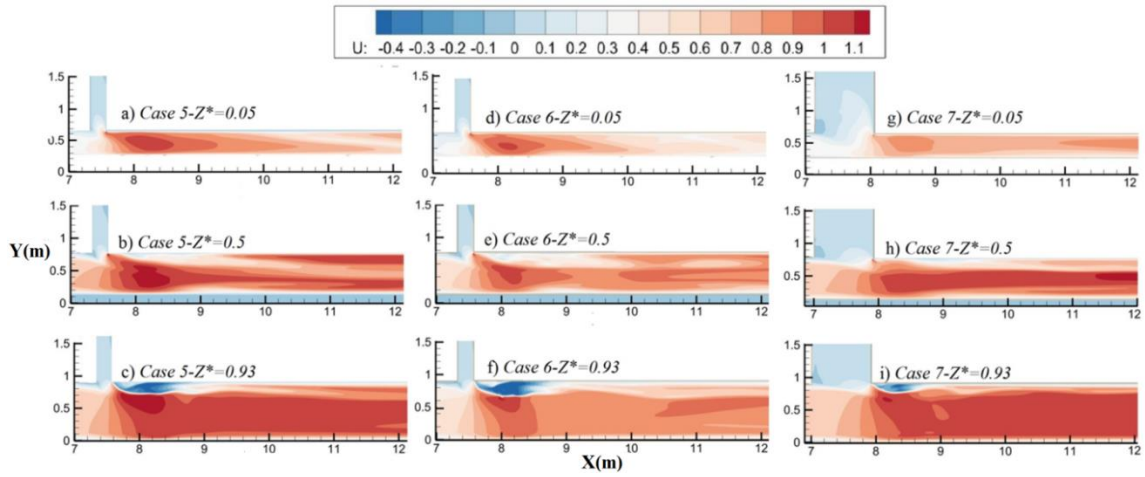

Figure 9. The distribution of the stream-wise component of velocity (U) in trapezoidal channel.

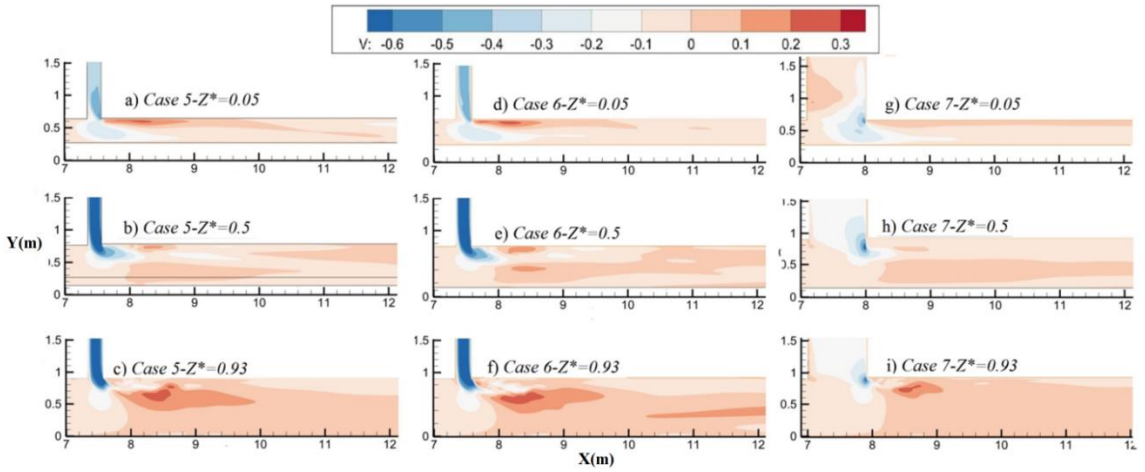

Figure 10. The distribution of the normal component of velocity (V) in trapezoidal channel.

Considering the effect of increasing the tributary channel width on the flow behavior, it could be noted that the length and width of the downstream recirculation zone decrease with increasing the width of the tributary channel. Besides, the area and extent of the U and V component of velocity in the high-velocity zone in the main channel decreases with increasing the tributary width. In addition, the width of the separating plate is significantly reduced by increasing the tributary width (see Figure 11c,i).

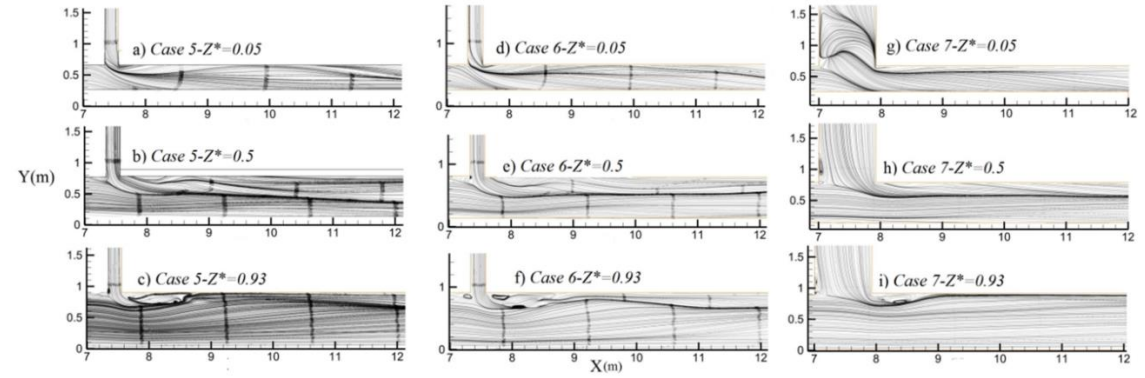

Figure 11. The effect of changing W* on the flow pattern at different elevations for trapezoidal channels.

On the other hand, the upstream stagnation zone formed in the tributary channel in case (7) is significantly larger and more intense compared to that in cases (5) and (6), covering up to 15% of the tributary width close to the water surface. It could also be inferred that it is larger and stronger near the surface compared to that formed in case (4) with a rectangular main channel.

3.2.2. Transverse Velocity Distribution and Flow Patterns

The cross-sectional velocity distribution and vertical structure are presented in Figures 12 and 13. A comparison of the flow structure in trapezoidal channels with that of rectangular channels shows significant differences either in the velocity distribution and the vertical structure. The negative velocity is observed in areas close to the surface adjacent to the inner bank of the channels. It could be inferred that the separation zone has a significantly different form from the classic recirculation zones in rectangular channels. In most cases, the width and the depth of the recirculation zone are almost equal. In fact, a fully-developed recirculation zone is absent in the trapezoidal channels [13]. Decreasing the upstream main flow discharge may result in the recirculation zone reaching the lower depths and the bed as well (Figures 12d and 1d). It also led to the increase in the surface and transverse area of the recirculation zone.

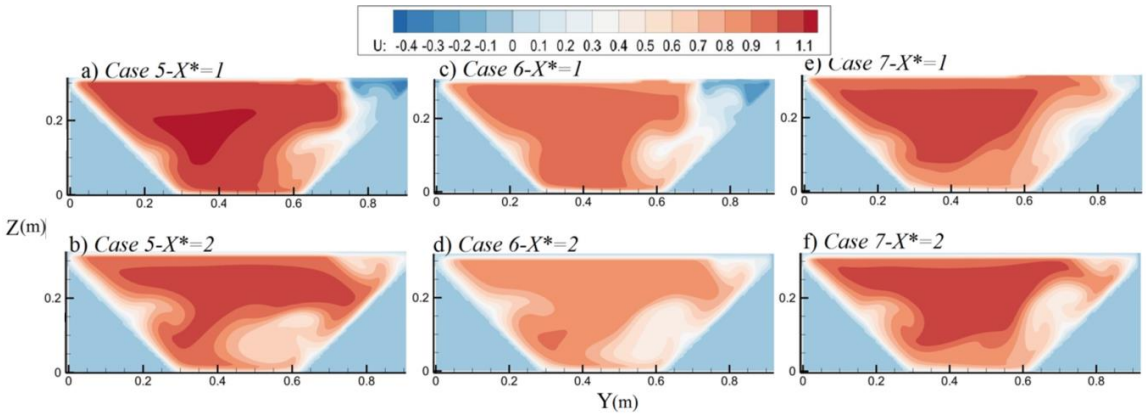

Figure 12. The effect of variations in W* and q* on the distribution of (U) in the transverse planes in the trapezoidal channel.

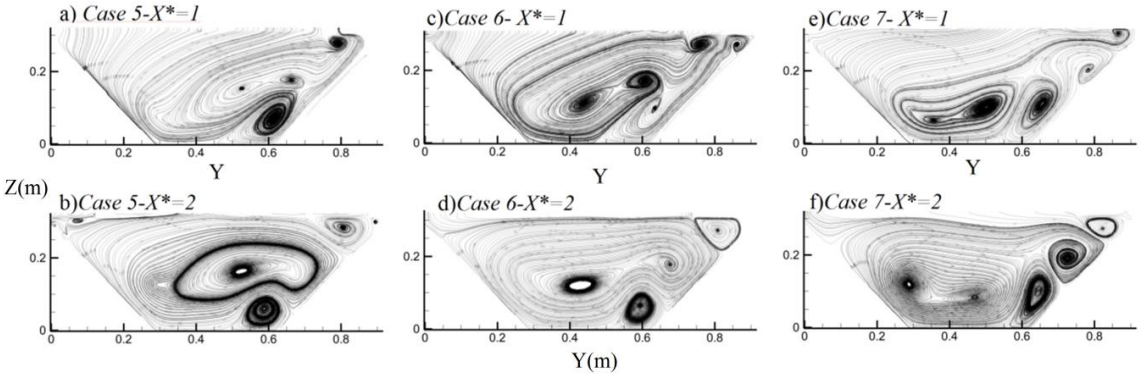

Figure 13. The effect of variations in W* and q* on flow patterns in the transverse plane in the trapezoidal channel.

Increasing the width of the tributary channel (W* = 1) resulted in a decreased maximum velocity zone in the main channel as well as a decreased absolute value of maximum velocity. It also led to the formation of a recirculation zone shallower and smaller than that of a narrower tributary channel of W* = 0.25 (Figure 12e,f and Figure 13e,f). Yet, increasing the tributary width resulted in the fastest development of helical movement along the channel centerline.

Figure 14 presents a 3D view of the flow behavior at confluences. Note that streamlines represent the flow from upstream main channels, and the colored ribbons are responsible for the tributary flow. Figure 14a presents the recirculation vortex's 3D formation in a rectangular channel, while Figure 14c presents the recirculation structure in the trapezoidal channel. The different structure and smaller size of the recirculation vortex in the trapezoidal channel is obviously indicated. Besides, the different behavior of the tributary flow at the confluence section is presented in Figure 14b,d. It is shown that a significant quantity of the tributary flow entering the rectangular main channel participates in the formation of the recirculation zone resulting in a large vortex. Additionally, an important portion of the flow moves upward and floats on the main channel suggesting the formation of the abovementioned surface roller. On the contrary, in the trapezoidal channel, the majority of the tributary flow slips downward over the bank slope, which prevents tributary flow to fully participate in the formation of the recirculation vortex. Hence, the surface currents of the main channel participate in the formation of the recirculation, resulting in an undeveloped and fully chaotic vortex. Furthermore, no portion of the tributary flow floats over the main flow, and in fact, the whole tributary flow moves downward, participating in the formation of the main spiral movement along the channel.

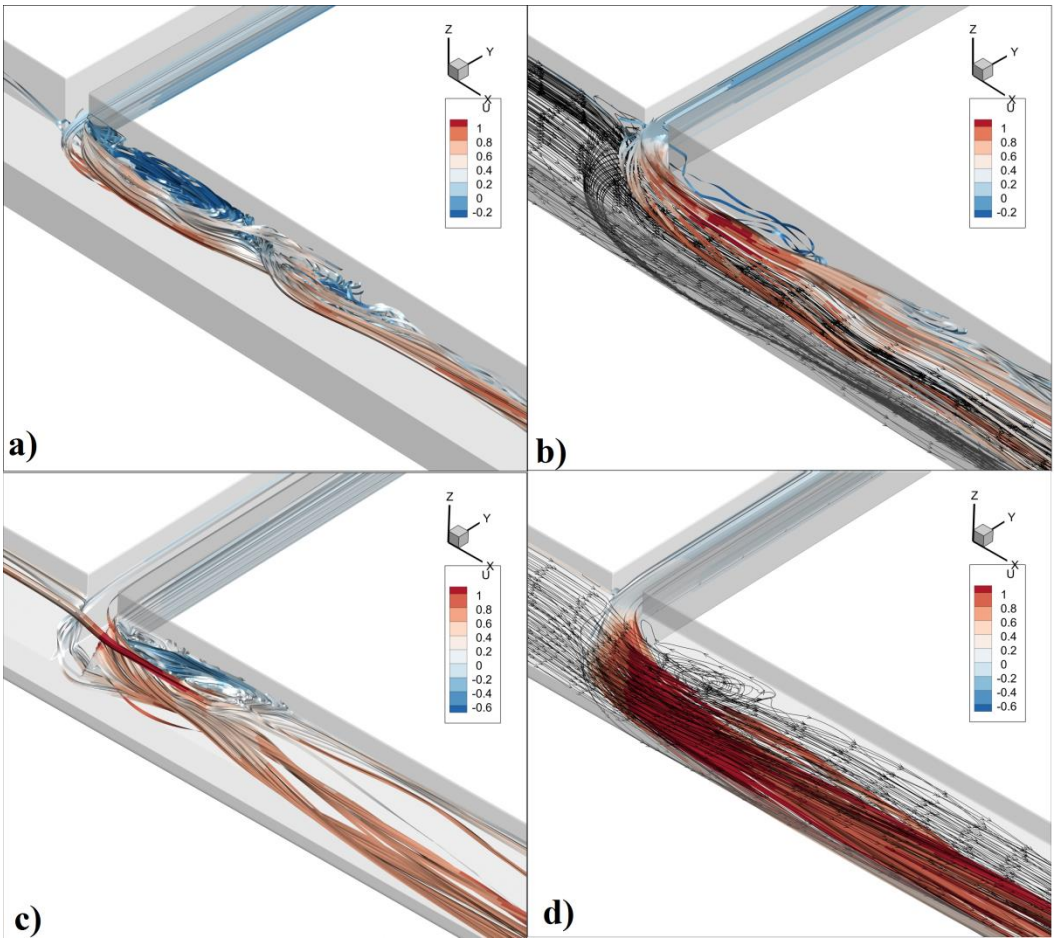

Figure 14. Three-dimensional streamlines at the confluences with W* = 0.25 and (**a**,**b**) rectangular and (**c**,**d**) trapezoidal geometry.

3.2.3. Bed Shear Stress

Figure 15 presents the transverse distribution of bed shear stress at the downstream corner of the confluence in trapezoidal and rectangular channels. It is indicated that the maximum value of τ in trapezoidal occurred in case (0) with q* = 0.25. It is evident that the bed shear stress increases

significantly when increasing the tributary discharge ratio from 0.25 (case (4)) to 0.75 (case (0)). It is also shown that increasing the tributary width ratio W* may reduce bed shear stress, which could result in smaller and more shallow scour holes.

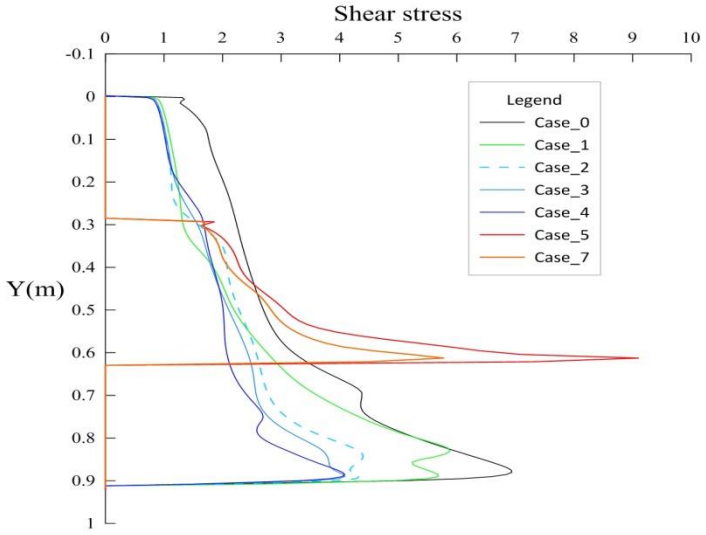

Figure 15. Bed shear stress for different cases.

Comparing the values of bed shear stress in the case of trapezoidal channels with those of rectangular channels, it could be inferred that the effect of variations in the discharge ratio or width ratio of tributary flow to main channel is more intense in the case of trapezoidal channels. Besides, the maximum value of bed shear stress in the case of trapezoidal channels is significantly higher than that in rectangular channels.

4. Conclusions

In this study, the effect of the ratio of the tributary to the main channel width on the flow structure in rectangular and trapezoidal channels at a confluence is discussed. Different conditions are modeled using a 3D CFD code, while results are compared to the experimental data from the literature. It is found that the width ratio (W*) has a significant effect on the flow structure and exchange of momentum between main and tributary flow at the confluence.

Generally, the flow structure in rectangular channels is different from that in trapezoidal channels, especially in the following points.

In rectangular channels, reducing the *W** ratio results in the formation of three main vortical zones in the main channel; (1) a large clockwise roller at the flow surface close to the outer wall of the main channel, (2) a counter-clockwise vortex adjacent to the bed tangent to the outer wall of the channel, and (3) a group of counter-wise vortices which form the main recirculation area. It is also concluded that the surface roller dissipates as the W* increases from 0.25 to 1. A fully developed recirculation zone forms in the main channel downstream of the confluence. The dimensions of the vortex increase with the decreasing W* and increase the momentum flux from the tributary. A reduced W* may result in the formation of stronger helical or spiral movements and more developed flow regions downstream of the confluence.

On the other hand, a fully developed recirculation zone is absent in cases with a trapezoidal channel. The formed recirculation zone suggests a non-uniform shape, which is most recognizable near the flow surface in different cases. It is also detached from the channel bed unlike rectangular channels. Increasing the width of the tributary channel may also lead to the formation of a recirculation zone shallower and smaller than that of a narrower tributary channel. Consequently, decreasing the upstream main flow discharge or increasing the W* ratio may lead the recirculation zone to touch the

lower depths and the bed as well in special cases with a small flow from the main channel. In such cases, the recirculation zone could be separated from the channel wall due to the complex upward movement of the main flow in collision with the outer wall of the channel.

Author Contributions: Investigation, supervision, project administration, funding, Writing—Review & Editing: Y.Z.; Methodology, Software, Writing—Original Draft Preparation, Formal Analysis, Data Curation: A.A.; All authors have read and agreed to the published version of the manuscript.

Funding: This research was funded by National Key Research and Development Program of China under No.2016YFC0401404.

Conflicts of Interest: The authors declare no conflict of interest.

Glossary

W_{sc}	Tributary Channel width
W_{mc}	Main channel width
W*	Width ratio (W_{sc}/W_{mc})
Q_{sc}	Tributary discharge
Fr_{mc}	Main channel Froude number
Fr_{sc}	Tributary Froude number
Fr*	Froude ratio (Fr_{sc}/Fr_{mc})
q*	discharge ratio

References

1. Constantinescu, G.; Miyawaki, S.; Rhoads, B.; Sukhodolov, A.; Kirkil, G. Structure of turbulent flow at a river confluence with momentum and velocity ratios close to 1: Insight provided by an eddy-resolving numerical simulation. *Water Resour. Res.* **2011**, *47*. [CrossRef]
2. Schindfessel, L.; Creelle, S.; De Mulder, T. How Different Cross-Sectional Shapes Influence the Separation Zone of an Open-Channel Confluence. *J. Hydraul. Eng.* **2017**, *143*, 04017036. [CrossRef]
3. Rhoads, B.L.; Sukhodolov, A.N. Field investigation of three-dimensional flow structure at stream confluences: 1. Thermal mixing and time-averaged velocities. *Water Resour. Res.* **2001**, *37*, 2393–2410. [CrossRef]
4. Best, J.L. Flow Dynamics At River Channel Confluences: Implications For Sediment Transport And Bed Morphology. *Recent Dev. Fluv. Sedimentol.* **1987**, 27–35. [CrossRef]
5. Biron, P.M.; Roy, A.G.; Best, J. Turbulent flow structure at concordant and discordant open-channel confluences. *Exp. Fluids* **1996**, *21*, 437–446. [CrossRef]
6. Gualtieri, C.; Ianniruberto, M.; Filizola, N. On the mixing of rivers with a difference in density: The case of the Negro/Solimões confluence, Brazil. *J. Hydrol.* **2019**, *578*. [CrossRef]
7. Gualtieri, C.; Filizola, N.; De Oliveira, M.; Santos, A.M.; Ianniruberto, M. A field study of the confluence between Negro and Solimões Rivers. Part 1: Hydrodynamics and sediment transport. *Comptes Rendus Geosci.* **2018**, *350*, 31–42. [CrossRef]
8. Mohammadiun, S.; Salehi Neyshabouri, S.A.A.; Naser, G.H.; Parhizkar, H.; Vahabi, H. Effects of open-channel geometry on flow pattern in a 90 junction. *Iran. J. Sci. Technol. Trans. Civ. Eng.* **2015**, *39*, 559–573.
9. Karami, H.; Farzin, S.; Sadrabadi, M.T.; Moazeni, H. Simulation of flow pattern at rectangular lateral intake with different dike and submerged vane scenarios. *Water Sci. Eng.* **2017**, *10*, 246–255. [CrossRef]
10. Taylor, E.H. Flow characteristics at rectangular open-channel junctions. *Trans. ASCE* **1944**, *109*, 893–902.
11. Webber, N.B.; Greated, C.A. An investigation of flow behaviour at the junction of rectangular channels. *Proc. Inst. Civ. Eng.* **1966**, *34*, 321–334. [CrossRef]
12. Shumate, E.D. Experimental Description of Flow at an Open-Channel Junction. Master's Thesis, University of Iowa, Iowa City, IA, USA, 1998.
13. Mignot, E.; Vinkovic, I.; Doppler, D.; Riviere, N. Mixing layer in open-channel junction flows. *Environ. Fluid Mech.* **2013**, *14*, 1027–1041. [CrossRef]
14. Zhang, T.; Xu, W.; Wu, C. Effect of discharge ratio on flow characteristics in 90° equal-width open-channel junction. *J. Hydrodyn. Ser. B* **2009**, *21*, 541–549. [CrossRef]

15. Zeng, C.; Li, C. A hybrid RANS-LES model for combining flows in open-channel T-junctions. *J. Hydrodyn.* **2010**, *22*, 154–159. [CrossRef]
16. Schindfessel, L.; Creelle, S.; De Mulder, T. Flow Patterns in an open channel confluence with increasingly dominant tributary inflow. *Water* **2015**, *7*, 4724–4751. [CrossRef]
17. Sharifipour, M.; Bonakdari, H.; Zaji, A.H.; Shamshirband, S. Numerical investigation of flow field and flowmeter accuracy in open-channel junctions. *Eng. Appl. Comput. Fluid Mech.* **2015**, *9*, 1–11. [CrossRef]
18. Ramos, P.X.; Schindfessel, L.; Pêgo, J.P.; De Mulder, T. Influence of bed elevation discordance on flow patterns and head losses in an open-channel confluence. *Water Sci. Eng.* **2019**, *12*, 235–243. [CrossRef]
19. Ramos, P.X.; Schindfessel, L.; Pêgo, J.P.; De Mulder, T. Flat vs. curved rigid-lid LES computations of an open-channel confluence. *J. Hydroinformatics* **2019**, *21*, 318–334. [CrossRef]
20. Azma, A.; Zhang, Y. The effect of variations of flow from tributary channel on the flow behavior in a T-shape confluence. *Processes* **2020**, *8*, 614. [CrossRef]
21. Wang, X.; Yan, X.; Duan, H.-F.; Liu, X.; Huang, E. Experimental study on the influence of river flow confluences on the open channel stage–discharge relationship. *Hydrol. Sci. J.* **2019**, *64*, 2025–2039. [CrossRef]